Analysis of Detector Calibrations for the GHRS for Cycles 4, 5 and 6

Howard H. Lanning, David R. Soderblom, Stephen J. Hulbert,
and Lisa E. Sherbert
May 22, 1997

ABSTRACT

This report presents the analysis of GHRS D1 and D2 detector calibrations encompassing Cycles 4, 5, and 6. Calibration tests examined include: dark count measurements, focus checks, flat-field count rates, sample mapping function, and line mapping function tests. Additional flat-field data from Cycles 1 to 3 were processed and displayed to demonstrate the continuing decreasing trend in the flat-field lamps response. Results of these analyses indicate the instrument has remained stable throughout the past three Cycles.

1. Introduction

Early in Cycle 4 a short series of calibration observations were begun in order to check out the instrument for routine science observations. Included among these tests were pulse height analysis/ion test/threshold adjustments, carousel commanding verifications, detector calibrations, spectral lamp tests, and G140L/Ech-A sensitivity measurements. This *Instrument Science Report* discusses the results of the analyses of the detector calibrations tests for the GHRS, based upon data from Cycles 4, 5, and 6.

The detector calibrations, nominally executed four times per year, are designed to monitor and verify the consistency of the instrument and identify new anomalies such as dead or noisy diodes, problems with background measurements, or peculiarities with the electronics.

Among the various calibration tests performed during the past three cycles are:

- dark count measurements
- focus checks at nominal high voltage and tweak current
- flat field exposures at the center of the photocathode
- coarse sample mapping function at the central *y* deflection
- coarse line mapping function at the central *x* deflection.

2. Procedure

The suite of detector calibration tests nominally include:

- *dark*: short-*x* dark photoscans (RAPIDs for Cycles 5 & 6)
- *focus:* long-*x* photoscans using the flat-field lamps with starting *x*-deflections ranging from 1622 to 1850 (spacing = 1) of the left edges of the photocathode mask at the nominal high voltage and tweak
- *flat-field:* short-*y* photoscan using the flat-field lamps at the center of the photocathode, producing 7 integrations centered around the nominal *y*-center
- *sample*: a series of four short-*x* photoscans of the left and right edges of the photocathode mask at the central *y* position of the photocathode
- *line*: a series of four short-*y* photoscans of the top and bottom edges of the photocathode mask at the central *x*-position of the photocathode.

3. Results

Data

The data sets analyzed in this study of the Cycles 4, 5, and 6 detector calibration tests are identified, along with the results, in the following Tables. These data are part of programs 5276 and 5546 (Cycle 4), 6172 and 6171 (Cycle 5), and 6898 and 6897 (Cycle 6). Both Side 1 and Side 2 observations were processed and examined. Additionally, flat-field data were re-examined for proposals 3298 (Cycle 1), 4068 (Cycle 2) and 5040 (Cycle 3) to provide a continuous trend analysis of the decreasing count rate noted in the OV/SV data and attributed to the flat-field lamps. Note that no Side 1 data during Cycles 1 to 3 were obtained as the detector was deactivated due to the Side 1 electronics failure.

Dark

Monitoring dark count calibration observations is one tool in monitoring the GHRS instrument health. Among the various potential contributing sources of background counts, including detector dark count, electrical interference within the GHRS or other devices, and effects caused by the charged particle radiation environment of the *HST* orbit, the dominant cause on-orbit is the effect of Cerenkov radiation bursts induced in the faceplate of the Digicon by cosmic rays The OV/SV observed dark rate was found to be very low, typically on the order of 0.005 counts sec^{-1} $diode^{-1}$ during the quiet period of the *HST* orbit when the observations were not influenced by SAA passages or geomagnetic latitude.

Calibrated data are input into the STSDAS/IRAF task **darksum** yielding count rates and statistical information. The **darksum** task combines the results of the **darkstat** and **hstpos** tasks to produce a report of count rate statistics and orbital position of *HST* at the time of the observations.

The mean count rate for the dark exposures throughout Cycles 4 to 6 has remained very near or just below the nominal mean count rate of 0.01 counts sec^{-1} $diode^{-1}$ noted in the *GHRS Instrument Handbook* and previously for the OV/SV data (see Tables 1 and 2). The mean dark count rate for Side 1 observations were 0.01, 0.008, and 0.0075 counts sec^{-1} $diode^{-1}$ for Cycles 4, 5, and 6, respectively. Side 2 mean count rates were 0.011, 0.012 and 0.013 counts sec^{-1} $diode^{-1}$ for Cycles 4, 5, and 6, respectively. Variations in these means relative to the means quoted in the handbook may, of course, be affected by orbital positioning of *HST*. No anomalies other than those identified in other GHRS ISRs during the past 3 Cycles are evident. During Cycles 5 and 6, the mode of observation employed RAPIDs as opposed to previously specified PHOTOSCANs. Consequently, a bad diode (#442) was not removed when using the **darksum** task in STSDAS/IRAF. As this diode influences the **darksum** output, a mask file was created to eliminate the offending diode and **gstat** was run in place of **darksum** to obtain the relevant means and standard deviations. No bad diodes were noted for Side 1 data in the **darksum** analyses.

Table 1. Side 1 Mean Dark Count Rate for Cycles 4 to 6

Rootname	Mean	σ	Comment
z25m0101t	0.006	0.025	Cycle 4
z25m0201t	0.0111	0.0333	
z25m0301t	0.0039	0.0197	
z25m0401t	0.0085	0.0291	
z25m0501t	0.0193	0.0437	
z2u90101t	0.0075	0.0869	Cycle 5
z2u91101t	0.0063	0.0798	
z2u92101t	0.0092	0.0963	
z3gy0101t	0.0069	0.0829	Cycle 6
z3gy1101t	0.008	0.0897	

Table 2. , Side 2 Mean Dark Count Rate for Cycles 4 to 6

Rootname	Mean	σ	Comment
z29w0101t	0.0109	0.0327	Cycle 4
z29w0201t	0.0148	0.0382	
z29w0301t	0.0088	0.0293	
z29w0401t	0.0123	0.0354	
z29w0501t	0.0073	0.0271	
z2ud0101t	0.0109	0.1047	Cycle 5
z2ud1101t	0.0113	0.1068	
z2ud2101t	0.0141	0.1194	
z2ud3101t	0.0157	0.1258	Cycle 6
z3jy1101t	0.0098	0.1011	

Focus

Focus is determined from a series of scans of the edge of the photocathode mask while the detector is illuminated by the flat-field lamp using observations of either the left or right photocathode edge. All observations are taken at the same *y*-deflection. The focus is taken to be the FWHM of the differential profile of the edge scan. Using the STSDAS/IRAF task **focusz** the data are merged into a single substepped image (1/8th diode-spaced image of the mask edge). The number of deflection steps between the points measuring the steep decline in count rate as the diode scans across the mask, i.e. between the 10% and 90% level, quantifies the focus. The theoretical "best" focus is 6.25 deflection steps. Each focus diode is 25×25 microns in size and each step is 6.25 microns, hence, there are 4 steps per diode. The values of the focus solutions for the Side 1 and Side 2 detectors are tabulated in Tables 3 and 4 below. No significant offsets are noted. Indeed, the focus has remained within ~2% of the best focus throughout Cycles 4 to 6.

Table 3. Side 1 Focus Check

Rootname	Defl Steps	YDEF	Voltage	Comment
z25m0202t	6.49	2048	21.6667	Cycle 4
z2u91201t	6.33			Cycle 5
z2u92201t	6.37			
z3gy0201t	6.37		21.5686	Cycle 6
z3gy1201t	6.37		21.6667	

Table 4. Side 2 Focus Check

Rootname	Defl Steps	YDEF	Voltage	Comment
z29w0202t	6.17	2048	21.9706	Cycle 4
z2ud0201t	6.21			Cycle 5
z2ud1201t	6.39			
z2ud2201t	6.26			
z2ud3201t	6.36			Cycle 6
z3jy1201t	6.39			

Flat Field

Flat fields are obtained by sampling the mean count rate for the seven bins of flat field spectra around the center of the photocathode and allow us to monitor the stability of the photocathode response/flatfield lamp combination. Included among the various uses for the flat fields are the calibration of the mapping functions and discriminator thresholds. While the intent of taking flat fields was never to ensure highly stable intensities or to provide precision radiometric standards, they do allow us a convenient source for count rate estimates. An example of one observed trend from previous analysis of the OV/SV data by

the IDT suggested the GHRS lamp count rates were decreasing at a rate of about 5% per year.

Tables 5 and 6 contain the mean count rate versus Modified Julian Date for Side 1 and Side 2, respectively, as determined by using the STSDAS/IRAF task **gstat.** These results are also represented graphically in Figures 1 and 2. The figures show a clear systematic trend of decreasing response in the flat field lamps. Between Cycle 1 and Cycle 6, the overall decrease of the D2 flat field lamp has been on the order of 12%, or about 2.4% per year. The D1 lamp has decreased by a similar amount.

Table 5. Side 1 Flatfield Mean Count Rates for Cycles 4 to 6

Rootname	Mean Count Rate	MJD (2400000+)	Comment
z25m0103t	4019	49418	Cycle 4
z25m0203t	3971	49467	
z25m0303t	3956	49655	
z25m0403t	3931	49776	
z25m0503t	3881	49895	
z2u91301t	3815	50083	Cycle 5
z2u92301t	3842	50205	
z3gy0301t	3790	50323	Cycle 6
z3gy1301t	3774	50412	

Table 6. Side 2 Flatfield Mean Count Rates for Cycles 1 to 6

Rootname	Mean Count Rate	MJD (2400000+)	Comment
z0p50n01t	1278	48488	Cycle 1
z0p51201t	1271	48790	
z1860103t	1256	48958	Cycle 2
z1860203t	1232	49041	
z1ig0203t	1218	49305	Cycle 3
z29w0103t	1202	49429	Cycle 4
z29w0203t	1192	49546	
z29w0303t	1180	49662	
z29w0403t	1176	49777	
z29w0503t	1157	49893	
z2ud0301t	1173	49972	Cycle 5
z2ud1301t	1160	50084	
z2ud2301t	1137	50202	
z2ud3301t	1126	50321	Cycle 6
z3jy1301t	1124	50412	

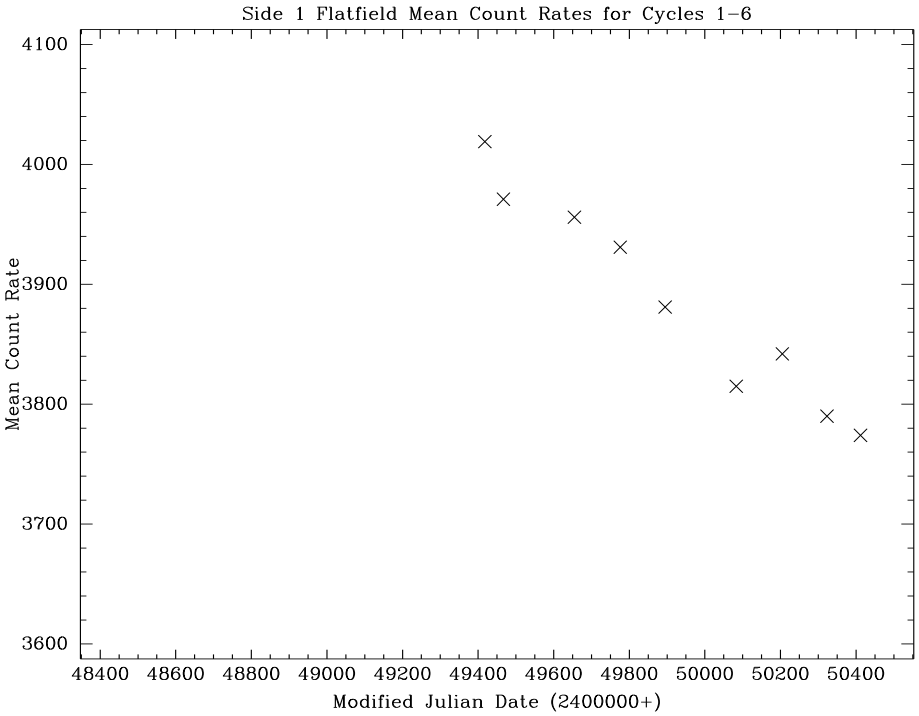

Figure 1: Side 1 flat-field mean count rates versus time.

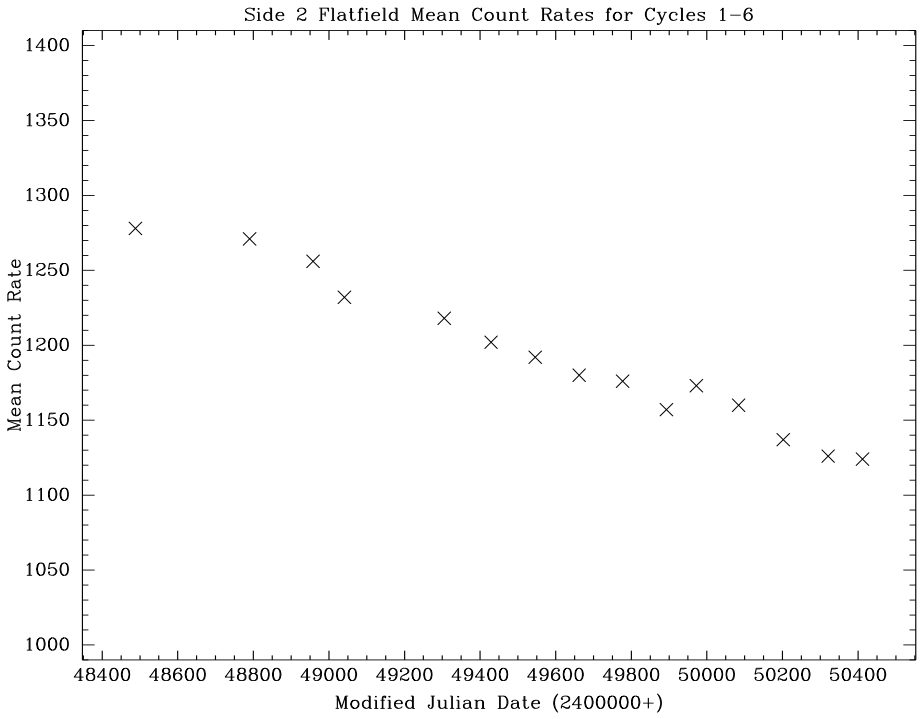

Figure 2: Side 2 flat-field mean count rates versus time.

The flat fields from Cycles 4 to 6 were also examined to verify that no unexpected or unexplained peculiarities remained after normalization. Adjacent flat fields were divided by each other and examined for uniformity and statistical errors. In this way, all known non-uniformities were removed, resulting in essentially a flat line with a small residual noise. Evidence of dead diodes which were identically zero and new or flaky diodes remained. No other gross photocathode peculiarities were detected. In all cases, the earlier flat field was divided by the next executed flat field. In each case the mean count level was slightly greater than 1.0 providing additional evidence of the continuing decrease in sensitivity of the flat field lamps. Bad diodes were eliminated in the statistical analysis of the normalized flats by setting upper and lower thresholds which removed those points from the solution. In Cycle 4, the resulting noise for Side 1 data was at the level of 0.7%, while the Side 2 data was ~1.3%. Cycles 5 and 6 were stable at ~1.3% for both detectors except in the case of the Side 1 flat field for Cycle 6. Due to an increased level of anti-coincidence events, excessive numbers of consecutive lines of bad science data were being flagged as bad shortening/terminating the exposures. Cycle 6 calibration exposure integration times were reduced in order to prevent excessive events and allow successful completion of the flat field exposures. System engineers suspect the cause was a noisy Side 1 flat field lamp. No further time-outs or terminated exposures occurred following the exposure changes.

Mapping Functions

Through the use of the magnetic deflection coils, the photoelectrons from a given point on the photocathode can be steered to any given diode for detection. Consequently, as noted in the Science Verification Report for GHRS, any particular physical diode can “see” photoelectrons from a wide range of positions on the photocathode. Sample and Line mapping functions of counts detected by the array of 500 science diodes may then be used to relate a specific diode to a discrete location on the cathode by solving the equations below, i.e., assigning a coordinate to the diode specified. Observations of this kind are used primarily for wavelength calibration but may also be used to note the positions of peculiarities in the photocathode response.

Sample Mapping

Observations of the left and right photocathode mask edges are used in determining the sample position, as a function of *x*-deflection and diode number. The location of the edges are computed by finding the position where the counts equal 1/2(min counts + max counts) about the edge: $S = S0 + B \times dx + E + D$, where

S is the sample position (can also be in 50 μm units with zero at left mask edge)
dx is the commanded *x*-deflection (minus 2048)
D is the diode position of the science diodes (the first science diode is 0)
S0, *B*, and *E* are the fitted sample mapping coefficients.

S0 is the sample coordinate of data recorded by the first science diode at the null *x* deflection (2048), and
B is a measure of the *x* deflection step size, nominally ~1/8 (0.125). The fitted coefficient *E* is the effective separation of the photocathode areas recorded by adjacent diodes.

Tables 7 and 8 list the computed sample mapping coefficients. These coefficients have remained stable and in good agreement with values quoted in the Science Verification Report. Any variations with the SV data were deemed insignificant and partly due to statistical errors in the measurements as well as thermal and magnetic effects.

Table 7. Side 1 Mean Sample Mapping Coefficients for Cycles 4 to 6

Prop ID	YDEF	B	S0	E	Comment
5276	2048	0.1256	31.61	1.0020	Cycle 4
6171		0.1259	31.75	1.0016	Cycle 5
6897		0.1257	31.73	1.0019	Cycle 6

Table 8. Side 2 Mean Sample Mapping Coefficients for Cycles 4 to 6

Prop ID	YDEF	B	S0	E	Comment
5547	2048	0.1241	28.75	1.0019	Cycle 4
6172		0.1249	29.77	1.0003	Cycle 5
6898/6172		0.1246	29.08	1.0012	Cycle 6

Line Mapping

Similar to the sample mapping, Line mapping relates the diode array position to a discrete *y* position on the photocathode. Edge positions are determined by constructing an edge profile as a function of *y*-deflection by summing the diodes between diode numbers 101 and 400. The computed coefficients are determined using the following equation: $L = L0 + A \times dy$, where

L is the line position (one unit = 50 μm on the photocathode; zero point is the upper mask edge)
dy is the commanded *y*-deflection (minus 2048)
L0 and *A* are the line mapping coefficients.

L0 is the line coordinate of data recorded by the first science diode at the null *y* deflection (2048). *A* is a measure of the *y* deflection step size, nominally 1/8 (0.125).

Tables 9 and 10 list the computed line mapping coefficients. The coefficients for Side 1 have also remained stable throughout Cycles 4 to 6 and are in good agreement with values quoted in the SV Report. The slight differences are, again, considered insignificant and

due primarily to statistical errors in the measurement of the data. However, examination of the values for Side 2 might suggest the presence of a small trend in the *A* coefficient, i.e. the y deflection step size. Solving the equation for a *y*-deflection of 500, for example, results in a difference of ~0.45 of a diode. Given the diode size of 50 μm, one might expect a shift of ~23 μ. This would suggest a displacement of the spectrum for the higher Echelle orders which could potentially allow the spectrum at this location to fall of the edge of the diode.

Table 9. Side 1 Mean Line Mapping Coefficients for Cycles 4 to 6

Prop ID	XDEF	A	L0	Comment
5672	2048	0.1262	214.01	Cycle 4
6171		0.1264	213.99	Cycle 5
6897		0.1264	214.07	Cycle 6

Table 10. Side 2 Mean Line Mapping Coefficients for Cycles 4 to 6

Prop ID	XDEF	A	L0	Comment
5547	2048	0.1237	224.82	Cycle 4
6172		0.1239	224.71	Cycle 5
6898/6172		0.1241	224.65	Cycle 6

4. Discussion

Exposure times were decreased for the Side 1 detector calibration tests in Cycle 5 and again in Cycle 6. An increased level of anti-coincident events resulted in the failure of several exposures due to too many lines of bad data. Engineering analysis suggests the cause may have been related to an instability in the D1 flat field lamp. The decreased exposure times (setting STEPTIME=0.2s) did indeed resolve the problem without the necessity of modifying detector thresholds.

5. Conclusions

Review of the detector calibration analysis suggests the detectors have remained stable overall and well characterized throughout the period of Cycles 4 to 6. Data for flat fields provides further evidence indicating the response for both flat field lamps continued to decline as expected following the trend detected with data as early as OV/SV.